J Mater Sci (2008) 43:2955–2961
DOI 10.1007/s10853-007-1750-3

Structures and purification of boron nitride nanotubes synthesized from boron-based powders with iron particles

Naruhiro Koi · Takeo Oku · Masahiro Inoue · Katsuaki Suganuma

Received: 6 March 2007 / Accepted: 6 April 2007 / Published online: 28 June 2007

Abstract Boron nitride (BN) nanotubes, nanohorns and nanocoils were synthesized by annealing Fe_4N/B, FeB and Fe/B powders at 1000 °C for 1–24 h in nitrogen gas atmosphere, and large amounts of BN nanotubes were obtained by annealing Fe_4N/B. The growth mechanism and atomic structures were investigated on cup-stacked BN nanotubes synthesized from Fe_4N/B by X-ray diffraction, high-resolution electron microscopy, electron diffraction and energy dispersive X-ray spectroscopy. As-produced BN soot was purified by removing non-BN nanomaterials such as metal catalyst particles and unreacted boron, and high purity BN nanotubes were obtained.

Introduction

Several studies have been reported on boron nitride (BN) nanomaterials such as BN nanotubes [1–3], nanocapsules [4, 5], nanoparticles [6], nanocable [7], and clusters [3]. Such materials are expected to be useful as electronic devices, high heat resistance semiconductors, insulator and lubricants because they provide excellent protection against oxidation and wear. Gas storage calculation of H_2 in boron nitride (BN) nanomaterials has also been reported [3]. However, selective synthesis and purification methods [8] are required to use them as ''devices''.

Recently, growth mechanisms of carbon nanotubes have been reported to optimize and control their structures to use for applications [9–12]. However, few experiments have been reported for BN nanomaterials, and understanding of their growth mechanism is important to achieve a controllable growth and to obtain a large amount of BN nanomaterials.

The purpose of the present work is to develop a new purification method and to investigate atomic structures of BN nanotubes. To understand growth mechanism of BN nanomaterials, Fe_4N/B, Fe/B, FeB, B was used as starting materials, and the structures of BN nanomaterials were compared. Most of synthesized samples contain a high amount of non-BN nanomaterials such as metal catalyst particles, boron and boron oxides. Therefore, it is necessary to purify the BN nanomaterials to characterize them appropriately. Purification experiments for carbon clusters have been carried out [13–16]. However, few experiments have been carried out for BN nanomaterials [8], and an efficient method for purification of BN nanomaterials is required. Although our research group has reported to eliminate Fe and B_2O_3 from as-produced soot, it is insufficient to eliminate unreacted boron and to obtain small size of BN nanomaterials [17]. The key steps in purification of BN nanomaterials in the present work would be HCl, HNO_3 and pyridine treatment. To investigate the growth mechanism and to confirm the formation of BN nanostructures, high-resolution electron microscopy (HREM) and energy-dispersive X-ray spectroscopy (EDX), which are powerful methods for atomic structure analysis, were carried out. Electron diffraction and X-ray diffraction (XRD) was also carried out to detect the reacted phases. These studies will give us a guideline for the synthesis of BN nanomaterials.

Experimental procedures

Four-types of mixture powders (Fe/B, FeB, Fe_4N/B and B) were used as starting materials for BN synthesis [18].

N. Koi · T. Oku (✉) · M. Inoue · K. Suganuma
Institute of Scientific and Industrial Research, Osaka University, Mihogaoka 8-1, Ibaraki, Osaka 567-0047, Japan
e-mail: oku-takeo@hotmail.co.jp

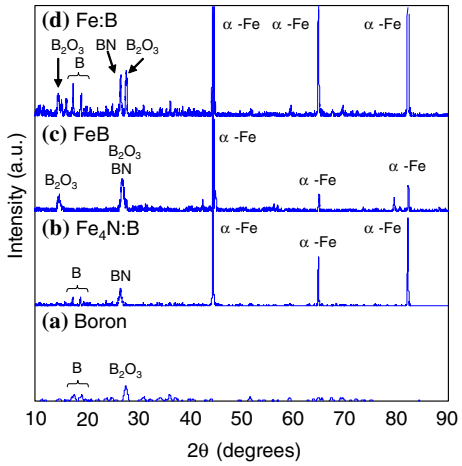

Fig. 1 X-ray diffraction patterns of (**a**) B, (**b**) Fe_4N/B, (**c**) FeB, and (**d**) Fe/B after annealing at 1000 °C for 1 h

Particle sizes of Fe (purity of 99.5%, Mitsuwa's Pure Chemicals, Osaka, Japan), FeB (99%, Kojundo Chemical Laboratory (KCL) Co. Ltd., Saitama, Japan), Fe_4N (99.9%, KCL) and B (99%, KCL) were about 5, 850, 50, and 45 μm, respectively. After Fe/B and Fe_4N/B (Weight ratio [WR] = 1:1, respectively) were well mixed in a triturator, the samples were set on an alumina boat and annealed in the furnace. The furnace was programmed to heat at 6 °C/min from a room temperature to 450, 700, and 1000 °C and hold for 1–24 h, and then cooled at 3 °C/min to a room temperature. Nitrogen pressure was 0.10 MPa, and its gas flow was 100 sccm.

As-produced soot synthesized from Fe_4N/B via the above method was purified by the following steps. The as-produced soot were poured in 4 M HCl solution and stirred for 4 h at a room temperature. The green color of the solution provides an indication of the dissolution of

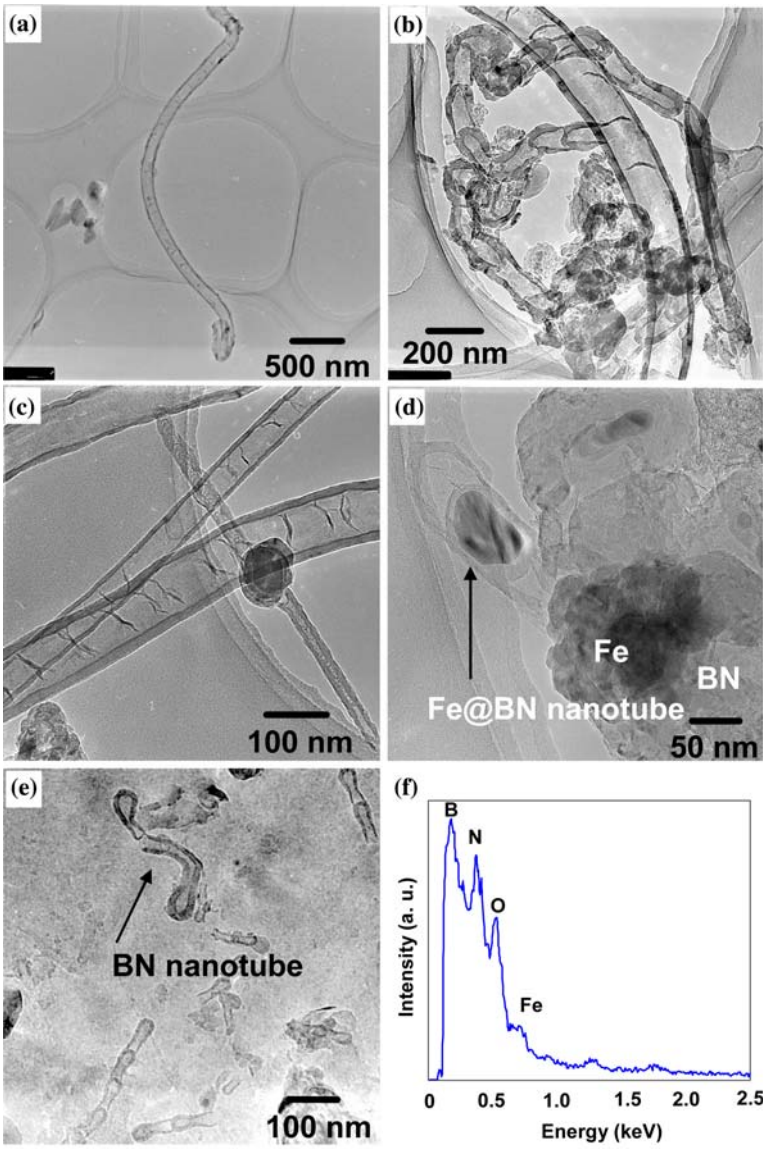

Fig. 2 TEM images of samples synthesized from (**a**) Fe/B, (**b**) FeB, and (**c**) Fe_4N/B. (**d**) Edge of boron of the samples Fe_4N/B after annealing, and (**e**) surface of boron after acid treatment. (**f**) EDX spectrum of (**d**)

Fe ions. After HCl treatment, the samples were poured in 1 M HNO_3 solution and stirred for 30 h at 50 °C. The yellow color of the solution provides an indication of the dissolution of boron. After both acid treatment, the solution was filtered and rinsed with deionized water until the pH of the filtrate became neutral and dried. Then, the samples were poured in pyridine to eliminate bulk BN, and high purity BN nanotubes with a cup-stacked structure were obtained by collecting supernatant.

Phases of the samples were determined by X-ray diffraction with Cu–Kα radiation. To observe the morphology of the samples, Transmission electron microscopy (TEM) and HREM observation were performed with a 300 kV electron microscope (JEM-3000F), and EDX analysis was performed using the EDAX system. For image processing of the observed HREM images, Digital Micrograph software (Gatan, CA, USA) was used. The digital images were masked and fast Fourier transformed. Basic structure models for BN nanotubes with a cup-stacked structure were constructed by CS Chem3D (CambridgeSoft, MA, USA). For stability calculations, structural optimization of the BN nanotubes with a cup-stacked structure was performed by molecular mechanics calculation (MM2). To compare observed images with calculated ones, HREM images were calculated by the multi-slice method using the MacTempas software (Total Resolution, CA, USA). The parameters used in the calculations are as follows: accelerating voltages = 300 kV, radius of the objective apertures = 5.9 nm^{-1}, spherical aberration C_s = 0.6 mm, spread of focus Δ = 8 nm, semi-angle of divergence a = 0.55 mrad, under defocus values Δf = –10 to –90 nm, unit cell (one cluster) = 5.0 × 5.0 × 12.0 nm^3, crystal thickness (unit-cell thickness, sixteen slices) t = 5.0 nm, space group *P*1 and assumed temperature factors of 0.02 nm^2.

Results and discussion

X-ray diffraction patterns of samples are shown in Fig. 1. Diffraction peaks of hexagonal BN and α-Fe were observed for each sample except for a sample synthesized from boron powder. Diffraction peaks of B_2O_3 were also observed for each sample except for a sample synthesized from Fe_4N/B powder. Figure 2a is a low magnification image of BN nanotubes synthesized from Fe/B. BN nanotubes were also observed from samples of FeB and Fe_4N/B as shown in Fig. 2b, c, respectively. For the sample of Fe_4N/B, BN nanotubes and Fe@BN nanotubes were formed at edge and surface of boron as shown in Fig. 2d, e, respectively. Figure 2(f) shows an EDX spectrum of edge of boron. In Fig. 2(f), EDX peaks of boron, nitrogen were observed, which showed the atomic ratio of B:N = 53.7:46.3, which indicates formation of BN at edge of boron. Peaks of Fe (0.70 keV) and oxygen were also

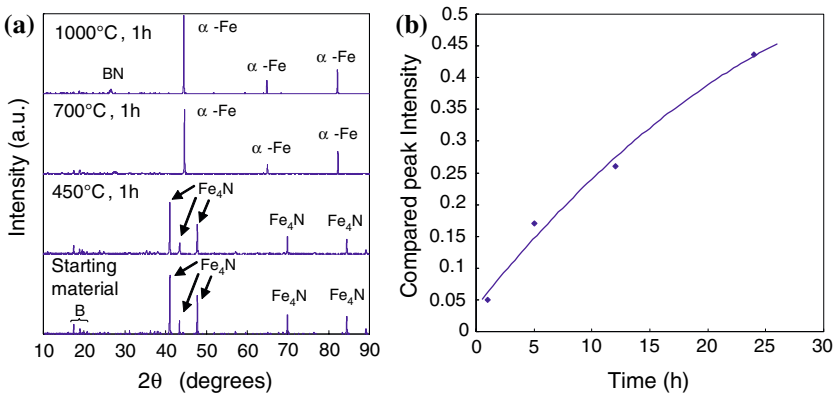

Fig. 3 (**a**) X-ray diffraction patterns of samples at elevated temperatures. (**b**) Intensity change of BN as a function of annealing time. (=peak of BN/Fe (No.1))

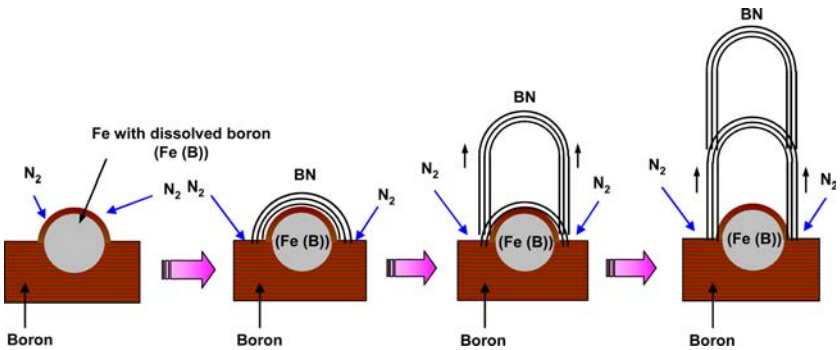

Fig. 4 Schematic illustration of the growth mechanism of BN nanotube

detected, which would be due to the formation of a small amount of B_2O_3. It is considered that Fe_4N/B is suitable to obtain high purity BN nanotubes from the results of Fig. 1 and 2. Therefore, X-ray diffraction patterns of samples synthesized from Fe_4N/B were investigated at various temperatures and time as shown in Fig. 3. In Fig. 3a, Fe_4N was reduced to Fe by boron at temperatures in the range of 450–700 °C, and BN was obtained at 1000 °C. Figure 3b shows intensity change of BN as a function of annealing time. A large amount of BN was obtained as time advances because Fe_4N would be sufficiently reduced to Fe.

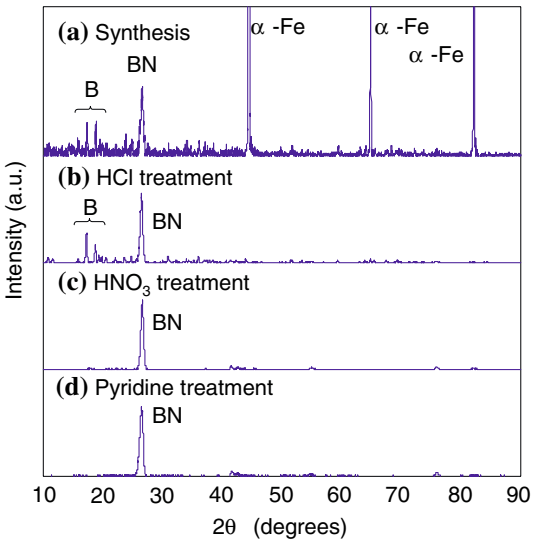

Fig. 5 X-ray diffraction patterns of samples after (**a**) synthesis, (**b**) HCl treatment, (**c**) HNO_3 treatment, and (**d**) pyridine treatment

Growth of carbon nanotubes was explained as a model of Vapor–Liquid–Solid (VLS) mechanism [19]. In this model, hydrocarbon such as methane is resolved in catalyst metal nanoparticles. Supersaturated solid solution of carbon in catalyst metal was precipitated as carbon nanotubes. BN nanotube growth might be explained in a similar model. Schematic illustration of a growth mechanism of a BN nanotube was proposed as shown in Fig. 4. Fe_4N was reduced to Fe by boron at 700 °C as shown in Fig. 3a, and Fe nanoparticles were dispersed and adhered on the surface of boron. Supersaturated solid solution of boron in Fe nanoparticles was formed and reacted with N_2 gas. BN nanotubes grow from these sites, and the diameter of nanotubes depends on particle size. Fe nanoparticles are easy to be separated from BN because Fe begins to react with BN from 1350 °C, and Fe@BN nanotubes were obtained as shown in Fig. 2d. Oriented BN nanotubes might be obtained when Fe nanoparticles are uniformly dispersed on surface of boron.

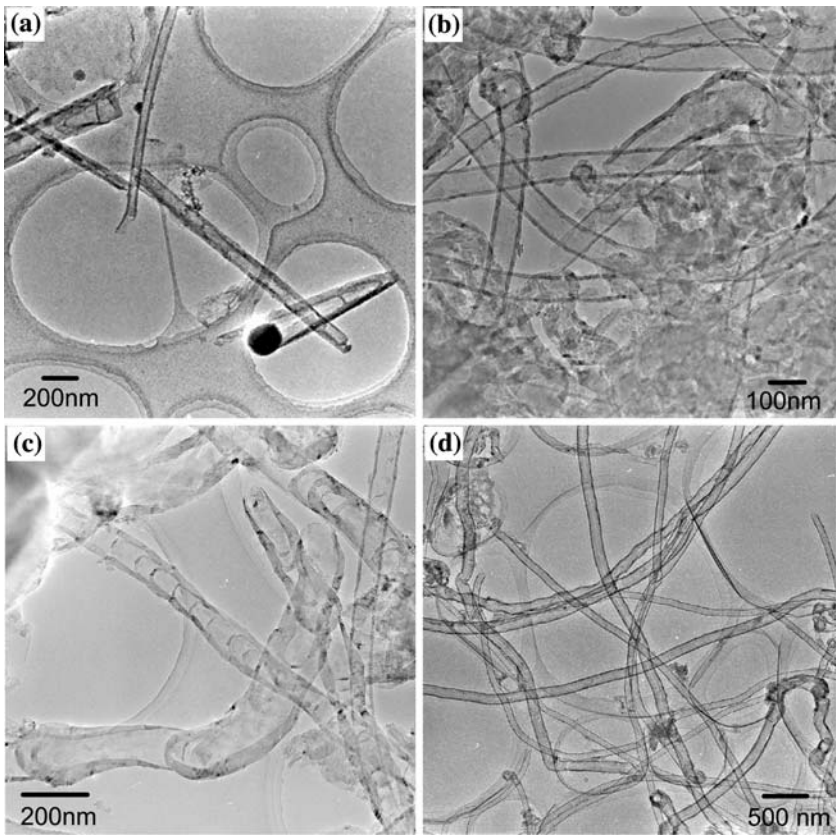

Fig. 6 TEM images of samples for each purification process. (**a**) as-produced soots, (**b**) after HCl treatment, (**c**) after HNO_3 treatment and (**d**) after pyridine treatment

X-ray diffraction patterns in a purification process are shown in Fig. 5. Diffraction peaks of hexagonal BN, boron and α-Fe are observed for the sample at annealed at 1000 °C for 1 h as shown in Fig. 5a. It is found that Fe was removed after HCl treatment as shown in Fig. 5b, and boron was removed after HNO_3 treatment as shown in Fig. 5c. After pyridine treatment, a strong peak of BN was obtained as shown Fig. 5d.

Figures 6 show TEM images of the samples for each process. There is no obvious change of the structure during the process, and BN nanotubes with small sizes were obtained after pyridine treatment. It is believed that bulk

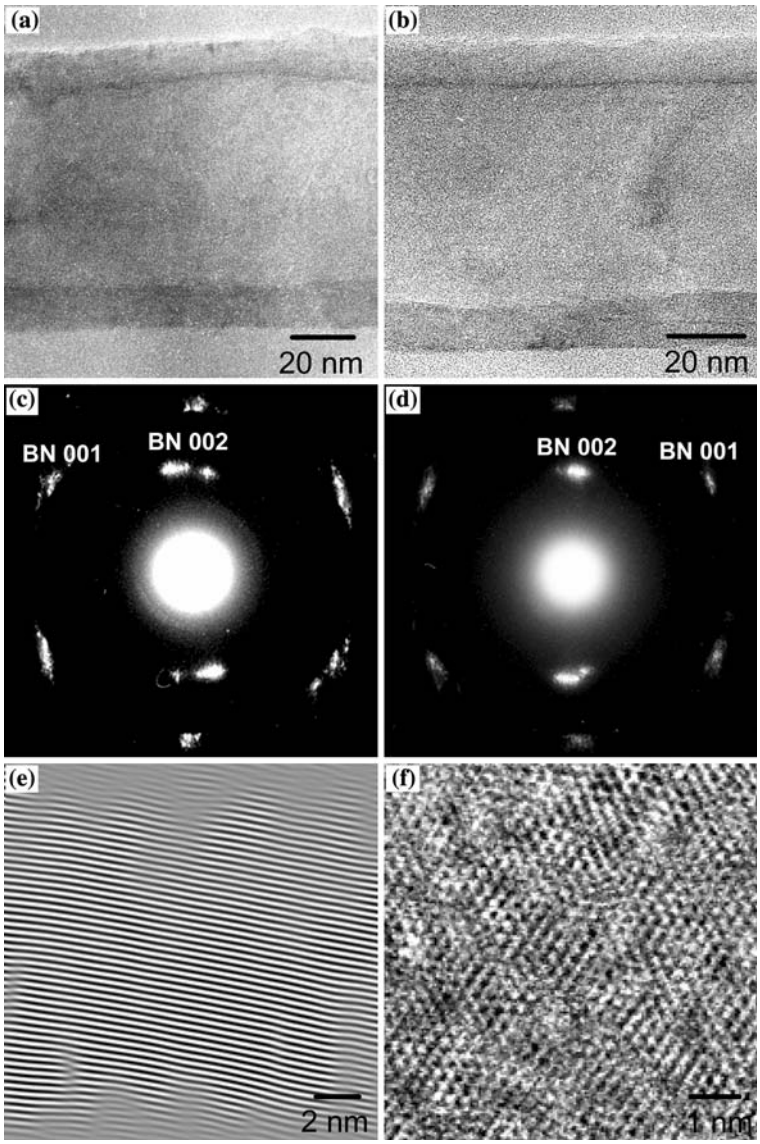

Fig. 7 TEM images of BN nanotubes with (**a**) a cup-stacked structure, and (**b**) a normal structure. Electron diffraction patterns obtained from (**a**) and (**b**), respectively. Fourier-filtered images of (**e**) side wall and (**f**) center of (**a**)

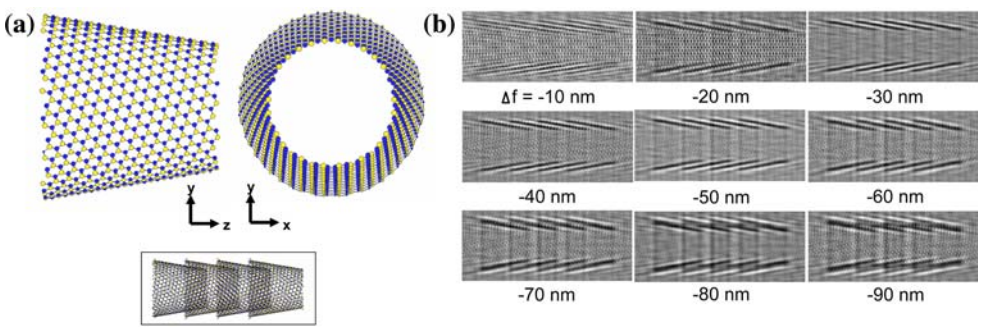

Fig. 8 (**a**) Structure model for $B_{565}N_{565}$. (**b**) Calculated HREM images of four-fold walled $B_{2240}N_{2240}$ nanotube with a cup-stacked structure as a function of defocus values

Table 1 Total energies of BN nanotubes with a cup-stacked structure by molecular mechanics calculation

	$B_{560}N_{560}$	$B_{1120}N_{1120}$	$B_{2240}N_{2240}$
Number of layers	1	2	4
Total energy [kcal/mol]	31.5	–287.9	–936.4
Total energy [kcal/mol·atom]	0.028	–0.129	–0.209

size of BN was eliminated and high purity BN nanotubes were obtained by pyridine treatment.

TEM images of BN nanotubes with a cup-stacked structure and normal BN nanotube after purification are shown in Fig. 7a, b, respectively. Electron diffraction patterns obtained from Fig. 7a, b are shown in Fig. 7c, d, respectively. 002 reflections of BN are inclined in Fig. 7c, which indicates that this BN nanotube has a cup-stacked structure, and the cone angle between the BN layers at both nanotube walls is ~22°. Strong peaks of BN nanotube in Fig. 7d corresponds to the plane of {002} of normal BN nanotube.

Fourier-filtered images of the side wall and the center of the BN nanotube are shown in Fig. 7e, f, respectively. BN nanotubes with a cup-stacked structure were formed by stacking of BN {002} layers for side walls, and hexagonal arrangements are observed at the center of the nanotube.

Figure 8a is a proposed structure model for $B_{565}N_{565}$ cup layer, which consists only of hexagonal BN rings. The nanotube axis is indicated by *z*-axis. A structure model and calculated HREM images of four-fold walled $B_{2240}N_{2240}$ nanotube with a cup-stacked structure are shown in Fig. 8b. The calculated image at defocus values at –40 nm agree with the HREM images in Fig. 7.

Total energies of $B_{565}N_{565}$, $B_{1120}N_{1120}$, and $B_{2240}N_{2240}$ cup-stacked BN layers calculated by molecular mechanics calculation are listed in Table 1. Distance between BN layers of nanotubes with a cup-stacked structure in a HREM image was measured to be ~0.35 nm, and the basic structure model was constructed based on it. After molecular mechanics calculations, the layer distances were optimized as ~0.38 nm. In addition, total energies of $B_{1120}N_{1120}$ and $B_{2240}N_{2240}$ were reduced by stacking of $B_{565}N_{565}$ nanotubes with a cup-stacked structure, and it is considered that the structure of BN multi-layered nanotubes with a cup-stacked structure would be stabilized by stacking hexagonal BN networks (molecular interaction).

Cone angles of BN cup-stacks were measured to be ~22°, which agreed well with that of the model in Fig. 8 (~22°). Although atomic structure models for BN nanotubes with a cup-stacked structure have been proposed from HREM observation and molecular mechanics calculations [20], we proposed a more suitable model in the present work.

Cone angles of carbon nanotubes with cup-stacked structures have been reported to be in the range of 45–80° [21, 22]. The cause of the different cone angles of the present cup-stacked BN nanotubes would be due to the different stacking of BN layers along *c*-axis (B–N–B–N...) from carbon layers.

Conclusion

BN nanotubes, nanohorns and nanocoils were synthesized by annealing Fe/B, FeB and Fe_4N/B powders at 1000 °C for 1–24 h in nitrogen gas atmosphere, and the growth mechanism of nanotubes were proposed from X-ray diffraction, HREM, and EDX analysis. Purification of BN nanotubes were carried out by HCl, HNO_3 and pyridine treatment to remove non-BN nanotubes such as metal catalysts, boron oxides and unreacted boron. Especially, bulks of BN were eliminated by pyridine treatment, and high purity BN nanotubes were obtained. An atomic structure models was proposed from HREM, and image simulations based on the proposed structure model agreed with experimental data. These unique structures would be suitable materials for gas storage, nanoelectronics devices and extreme environmental materials with excellent protection against oxidation and wear.

Acknowledgements The authors would like to thank Dr. I. Narita for experimental help and warm encouragement.

References

1. Mickelson W, Aloni S, Han W-Q, Cumings J, Zettl A (2003) Science 300:467
2. Golberg D, Xu F-F, Bando Y (2003) Appl Phys A 76:479
3. Oku T, Narita I, Nishiwaki A, Koi N (2004) Defects and Diffusion Forum 226–228:113
4. Oku T, Hirano T, Kuno M, Kusunose T, Niihara K, Suganuma K (2000) Mater Sci Eng B 74:206
5. Narita I, Oku T, Tokoro H, Suganuma K (2006) Solid State Commun 137:44
6. Oku T, Hiraga K, Matsuda T, Hirai T, Hirabayashi M (2003) Diam Relat Mater 12:1918
7. Oku T, Koi N, Narita I, Suganuma K, Nishijima M (2007) Mater Trans 48 (in press)
8. Zhi C, Bando Y, Tang C, Honda S, Sato K, Kuwahara H, Golberg D (2006) J Phys Chem B 110:1525
9. Emrah Unalan H, Chhowalla M (2005) Nanotechnology 16:2153
10. Kusunoki M, Honjo C, Suzuki T, Hirayama T (2005) Appl Phys Lett 87:103
11. Ding F, Rosén A, Bolton K (2005) Carbon 43:2215
12. Ikuno T, Honda S, Kamada K, Oura K, Katayama M (2005) J Appl Phys 97:104329-1-4
13. Niyogi S, Hu H, Hamon MA, Bhowmik P, Zhao B, Rozenzhak SM, Chen J, Itkis ME, Meier MS, Haddon RC (2001) J Am Chem Soc 123:733

14. Georgakilas V, Voulgaris D, Vázquez E, Prato M, Guldi DM, Kukovecz A, Kuzmany H (2002) J Am Chem Soc 124:14318
15. Chattopadhyay D, Galeska I, Papadimitrakopoulos F (2002) Carbon 40:985
16. Gregan E, Keogh SM, Maguire A, Hedderman TG, Neill LO, Chambers G, Byrne HJ (2004) Carbon 42:1031
17. Koi N, Oku T, Narita I, Suganuma K (2005) Diam Relat Mater 14:1190
18. Narita I, Oku T, Tokoro H, Suganuma K (2006) J Electron Microsc 55:123
19. Ogrin D, Colorado R Jr, Maruyam B, Pender MJ, Smalley RE, Barron AR (2006) Dalton Trans 229:229
20. Oku T, Narita I, Nishiwaki A (2006) J Euro Ceram Soc 26:443
21. Endo M, Kim YA, Hayashi T, Fukai Y, Oshida K, Terrones M, Yanagisawa T, Higaki S, Dresselhaus MS (2002) Appl Phys Lett 80:1267
22. Endo M, Kim YA, Hayashi T, Yanagisawa T, Muramatsu H, Ezaka M, Terrones H, Terrones M, Dresselhaus MS (2003) Carbon 41:1941